RSC Pharmaceutics

ROYAL SOCIETY OF CHEMISTRY

PAPER

View Article Online
View Journal | View Issue

Cite this: *RSC Pharm.*, 2024, **1**, 755

Acid- and base-resistant antimicrobial hydrogels based on polyoxometalates and chitosan†

Callum McWilliams,[a,b] Isabel Franco-Castillo,[a,b] Andrés Seral Ascaso,[a,b] Sonia García-Embid,[a,b] Mariella Malefioudaki,[a,b] Johann G. Meier,[c] Rafael Martín-Rapún[a,b] and Scott G. Mitchell*[a,b]

Invasive fungal infections kill more than 1.7 million and affect over a billion people each year; however, their devastating impact on human health is not widely appreciated and frequently neglected by public health authorities. In 2022, the WHO highlighted the urgent need for efficient diagnostic tests as well as safe and effective new compounds, drugs, and vaccines. Our hypothesis was that the naturally occurring polymer chitosan (CS) could be combined with molecular polyoxometalates (POMs) to produce POM@CS hybrid materials to promote broad-spectrum activity and habilitate synergic effects, which will ultimately help to prevent the appearance of resistances. Here we report the synthesis, characterisation, and antimicrobial activity of POM@CS hydrogels. Spectroscopic (FT-IR & EDS) and electron microscopy (SEM & TEM) techniques revealed the structural composition and morphology of the hybrid materials, whilst dynamic mechanical analysis demonstrated that the mechanical properties of the hydrogels were stable between pH 2 and 10 and were highly resistant to acidic conditions. The POM@CS hydrogels were active against Gram-positive *Bacillus subtilis* and Gram-negative *Escherichia coli* bacteria, and proved to completely reduce fungal growth of *Aspergillus niger* and *Cladosporium cladosporioides*. Furthermore, the antimicrobial activity of the hydrogels could be enhanced through the inclusion of naturally occurring antimicrobial agents such as eugenol and cinnamaldehyde. Altogether, the development of such surface-active antimicrobial hydrogels pave the way to functional materials that can prevent biofilm formation in health and environmental applications and contribute to reducing the spread of antimicrobial resistance.

Received 29th February 2024,
Accepted 16th May 2024

DOI: 10.1039/d4pm00062e

rsc.li/RSCPharma

Introduction

Only a few decades ago, antimicrobial resistance (AMR) was largely confined to hospitals and long-term care facilities, but over the last decade, it has emerged as a serious threat to global public health. In May 2014, the 67th World Health Assembly adopted resolution WHA67.25 on antimicrobial resistance, in which it requested to develop a global action plan to combat AMR.[1] In 2021, the "*Call to Action on Antimicrobial Resistance*" was launched, in which members committed to keeping AMR high on the political agenda, build awareness and understanding, and strengthening coordination, political leadership, and collaboration on AMR actions.[2] This included the correct use of antibiotics, administration of a correct dose for the appropriate duration, with the aim of reducing the prevalence of AMR.[3]

However, since the COVID-19 pandemic began four years ago, there has been a rise in AMR due to an increased incidence of antibiotic prescriptions for COVID-19 patients.[4] Worryingly, it has been demonstrated that in China over 71% of adult patients hospitalised with COVID-19 received administered antibiotics despite a bacterial co-infection rate of only 1%.[5,6] The pandemic has also led to a prolonged and significant use of disinfectants to mitigate the spread of SARS-CoV-2 and other opportunistic pathogens. Currently, almost 50% of the products listed by the U.S. Environmental Protection Agency (EPA) as effective against SARS-CoV-2 contain quaternary ammonium compounds (QACs).[7]

The antimicrobial properties of quaternary ammonium compounds were discovered in the early part of the twentieth century and little subsequent innovation has been achieved. The mode of action of QACs is based on a common mechanism in which the cationic head is attracted to the anionic charge of the bacterial membrane, followed by the insertion of

[a]*Instituto de Nanociencia y Materiales de Aragón (INMA), CSIC-Universidad de Zaragoza, 50009 Zaragoza, Spain. E-mail: scott.mitchell@csic.es*
[b]*CIBER de Bioingeniería, Biomateriales y Nanomedicina, Instituto de Salud Carlos III, 28029 Madrid, Spain*
[c]*ITAINNOVA – Instituto Tecnológico de Aragón, Calle María de Luna, no. 7, Zaragoza, 50018, Spain*

†Electronic supplementary information (ESI) available: Additional materials characterisation and antimicrobial data. See DOI: https://doi.org/10.1039/d4pm00062e

a non-polar tail into the lipid bilayer, which reduces the structural integrity of the bacterial membrane producing lysis and cell death.[8–10] It was considered that, with such a non-specific mechanism of action, QAC-based compounds would innately evade the development of resistance; nevertheless, bacterial tolerance and genetic resistance to QACs emerged as early as the 1980s.[11,12] Subsequent studies across Gram-negative and Gram-positive bacteria have shown that resistance to QACs developed primarily through biofilm formation, alterations to the membrane, and production of efflux systems.[13–15] Moreover, through horizontal gene transfer these traits have rapidly spread, leading to an increasing resistance to QAC treatments in clinical isolates. Troublingly, the use of sub-inhibitory concentrations of QAC treatments have even been shown to promote the co-resistance to antibiotics through the selective pressure for the spread of resistant plasmid-encoding AMR genes.[16,17] Thus the global widespread use of disinfectants and antibiotics stimulated by the COVID-19 pandemic has heightened concern about accelerated antibiotic resistance.[18]

There is now a concerted effort by research communities to develop new antibacterial agents in an attempt to combat AMR; however fungal pathogens represent an underestimated class of microbes that have been severely overlooked by researchers and healthcare authorities.[19–21] Fungi cause diverse diseases in humans, ranging from allergic syndromes to superficial, disfiguring and life-threatening invasive fungal diseases (IFDs), which together affect more than a billion people worldwide.[22] Historically, treatment has relied heavily on just four classes of systemically acting antifungal drugs: polyenes, azoles, echinocandins and the pyrimidine analogue 5-flucytosine, all of which are encountering resistance; particularly in immunocompromised patients.[23] In 2022, the World Health Organisation (WHO) published a report highlighting the first-ever list of fungal "priority pathogens" – a catalogue of the 19 fungi that represent the greatest threat to public health. The WHO fungal priority pathogens list (FPPL) is the first global effort to systematically prioritise fungal pathogens, considering the unmet research and development needs and the perceived public health importance. The WHO FPPL aims to focus and drive further research and policy interventions to strengthen the global response to fungal infections and antifungal resistance.[24]

Recent research has demonstrated that polyoxometalate-based materials can be used to kill, remove, or prevent the growth of microorganisms in different environments and settings.[28–36] Polyoxometalates (POMs for short) are a diverse class of nanoscale molecular metal oxides, characterised by a wide and versatile range of physicochemical properties that can be tuned on the molecular level.[25] Their redox properties and high oxidation activity also make them useful to a wide variety of applications, from catalysis[26] to medicine.[27] The rich redox chemistry and diverse oxidation states of POMs means they also display antimicrobial activity: they cross lipid membranes, interact with proteins and DNA, and are producers of reactive oxygen species (ROS).[28] Recent research has demonstrated that POM-based materials can be used to kill, remove, or prevent the growth of microorganisms in different environments and settings.[29–36] Our hypothesis is that POMs can be hybridised with the naturally occurring polymer chitosan to yield hydrogels that provide potent antifungal activity.

Chitosan is a linear mucopolysaccharide composed of β-(1→4)-linked D-glucosamine (deacetylated unit) and *N*-acetyl-D-glucosamine (acetylated unit) glycosidic bonds.[37] It is derived from the deacetylation of chitin – the second most naturally abundant biopolymer after cellulose – a structural material found in the exoskeleton of crustaceans and insects, and the cellular walls of fungi.[38] Chitosan is cationic due to the presence of its amino groups, with a pK_a of 6.5. It is one of the most extensively used and affordable natural polysaccharides, where its biodegradability, nontoxicity, biocompatibility, and antimicrobial activity make it a material of choice for bioapplications.[39,40]

Our objective was to investigate the physicochemical and antimicrobial properties of hybrid hydrogels prepared from Keggin-type POMs and chitosan. We hypothesised that such POM@CS hydrogels could be functionalised (or doped) with known antimicrobial agents, which would improve the antimicrobial properties already exhibited by the original hydrogels. We also reasoned that the use of POMs with high negative charge would enhance the acid- and base-resistant properties of chitosan hydrogels *via* ionic and hydrogen-bonding crosslinking interactions with the polysaccharide. To test these hypotheses, the antibiofilm activity of the hydrogels was tested against model bacterial and fungal strains, and the acid and base-resistant properties of the hydrogels were evaluated. Such hybrid materials could find application as resistant surface-active materials for health and environmental applications, for example as adhesive transdermal patches for fungal infections, or as novel and efficient adsorbents as part of composite membranes with antifouling properties for the treatment of acidic wastewater.

Results and discussion

Synthesis of polyoxometalate–chitosan hydrogels (POM@CS)

Monolacunary Keggin-type POM $[SiW_{11}O_{39}]^{8-}$ was synthesised according to literature protocols. Keggin-type POMs have the general formula $[XM_{12}O_{40}]^{q-}$, where the heteroatom X can be a p-block element (*e.g.*, Si(IV), As(V), Ge(IV) or P(V)) and the addenda metal M is d-block element such as W(VI), Mo(VI) or V(V).[41] Keggin POMs are constructed with a central XO_4 tetrahedron surrounded by twelve MO_6 octahedra. $[MO_x]^{y-}$ units can be removed through acid hydrolysis resulting in the formation of lacunary POMs with vacant metal binding sites. These vacant sites can be filled with divalent transition metals, such as Co(II), Cu(II), and Zn(II). Transition-metal substituted POMs can be further transformed by the addition of functional groups at the transition metal.[42]

The negatively charged polyoxometalates were used to form composite chitosan hydrogels through ionic crosslinking inter-

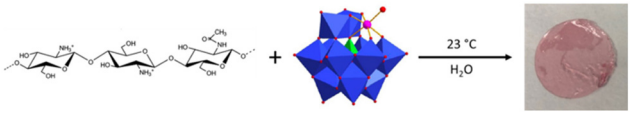

Fig. 1 Overview of the general synthetic approach showing the synthesis of the $CoSiW_{11}$@CS hydrogel from aqueous solutions of chitosan and the monosubstituted Keggin $K_6[Co(H_2O)SiW_{11}O_{39}]$ at room temperature.

actions. The POM@CS hydrogels were prepared in 24-well plates at room temperature by adding 5 mM aqueous solution of the corresponding POM, which acts as a gelling agent, to 35 mg mL^{-1} of chitosan (Fig. 1). The ionic gelation process was completed within a few minutes; however, all hydrogels were left to stand for 24 h before being characterised and used for further studies. The corresponding hydrogels possessed a diameter of 18 mm and thickness of 50 μm. POM@CS gels were prepared using $K_8[SiW_{11}O_{39}]$ and $K_6[M(H_2O)SiW_{11}O_{39}]$, where M = Co(II), Cu(II), and Zn(II). For simplicity, the results described herein focus on POM@CS hydrogels developed using the monosubstituted dodecatungstosilicate Keggin-type POM, $K_6[Co(H_2O)SiW_{11}O_{39}]$, which will henceforth be referred to as $\{CoSiW_{11}\}$. Transition metal-substituted POMs were deployed to enhance the gelation process and further strengthen the hybrid hydrogels, since the substituted metals (Co, Cu, or Zn) can coordinate to amine functional groups on chitosan.

Characterisation of POM@CS

The chemical composition of $CoSiW_{11}$@CS was investigated using Fourier transform infrared spectroscopy (FT-IR) and compared to the FT-IR spectra of the corresponding $\{CoSiW_{11}\}$ single crystals and the chitosan solution (Fig. 2). The broad band found at 3300 cm^{-1} in the $CoSiW_{11}$@CS hydrogel spectrum can be attributed to the O–H and N–H stretching, from the chitosan. The sharp band at 1600 cm^{-1} was associated with the primary amide vibration from the chitosan and H_2O from the POM. The small peak at 1400 cm^{-1} corresponded to the methylene groups ($-CH_2$) in the chitosan solution, and similarly, the stretch at 1375 cm^{-1} was attributed with the methyl groups ($-CH_3$). The band at approximately 1100 cm^{-1} was due to the antisymmetric C–O–C stretching and C–N stretching from the chitosan. The peaks at 990, 950 and 900 cm^{-1} in the $CoSiW_{11}$@CS hydrogel spectrum are identified in that of the $K_6[Co(H_2O)SiW_{11}O_{39}]$ POM and can be attributed to the asymmetric stretching of W═O, W–O and W–O–W, respectively.[43]

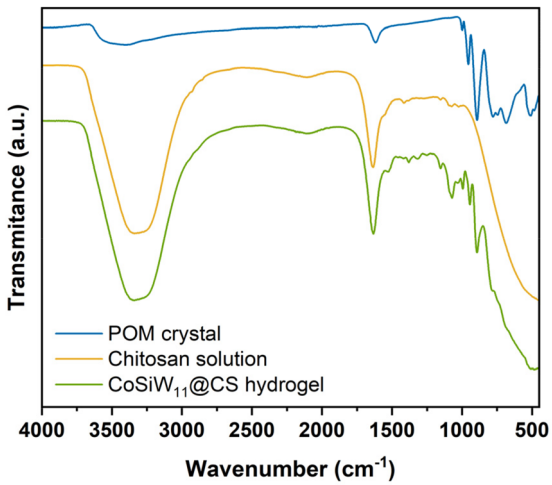

Fig. 2 FT-IR spectra of $K_6[Co(H_2O)SiW_{11}O_{39}]$ single crystals, chitosan solution, and the corresponding $CoSiW_{11}$@CS hydrogel.

Scanning electron microscopy (SEM) was used to obtain high-resolution images of the $CoSiW_{11}$@CS hydrogels (Fig. 3). Under high vacuum conditions of SEM, the hydrogel matrix can be seen to be composed of interlinked $CoSiW_{11}$@CS fibres which supports ionic crosslinking interactions.

The fibrous nature of the gels was observed more clearly using transmission electron microscopy (TEM), by accelerating a high-voltage particle beam of electrons through a thin sample of hydrogel. Since thin samples were required, the typical hydrogel samples could not be used. Instead, the TEM grid was immersed in the 35 mg mL^{-1} chitosan solution before then being immersed in the 5 mM $\{CoSiW_{11}\}$ solution to synthesise the hydrogels *in situ* on the TEM grid. Fig. 4 shows the TEM images obtained from this carbon-coated Cu TEM grid containing *in situ* assembled $CoSiW_{11}$@CS. The morphology of the sample was commensurate with the SEM images (Fig. 3), where a uniform dispersion of the hydrogel matrix was visible throughout (refer also to Fig. S2†).

The chemical composition of the $CoSiW_{11}$@CS hydrogel was verified using through Energy-Dispersive X-ray Spectroscopy (EDS). The transitions of the electrons for each

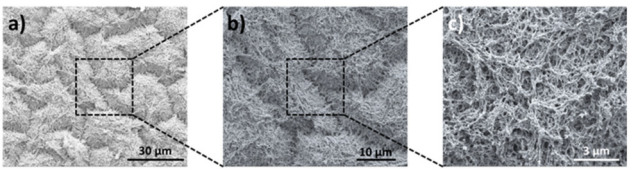

Fig. 3 SEM imaging shows the composition and topography of the $CoSiW_{11}$@CS hydrogel at: (a) 1500x; (b) 5000x; and (c) 50 000x magnification.

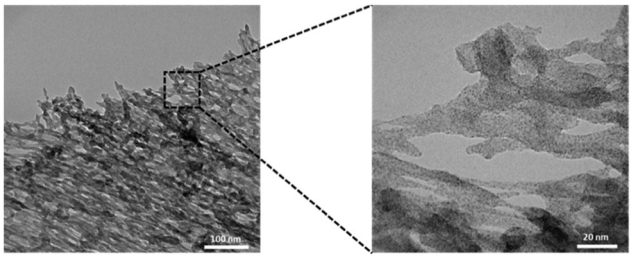

Fig. 4 Structure and morphology of $CoSiW_{11}$@CS observed by TEM.

element were as follows: O – $K\alpha_1$, Co – $K\alpha_1$, Si – $K\alpha_1$, and W – $L\alpha_1$, where the Kα notation refers to the X-ray emitted when an electron from the K shell is replaced by an electron from the next closest shell (L), similarly, Lα notates the X-ray emitted when an electron in the M shell (the next closest shell) replaces an electron from the L shell. Fig. S3† highlights the homogeneous dispersion of $\{CoSiW_{11}\}$ throughout the $CoSiW_{11}$@CS hydrogel, while the corresponding EDS spectrum confirmed the composition (Fig. S4†).

Acid- and base-resistance of POM@CS

Traditional hydrogels cannot maintain their structure in both acidic and alkaline solution environments due to the highly corrosive properties of acid and alkali solutions, which can penetrate into the hydrogel network, resulting in irreversible damage to the hydrogel structures. Under strong acid or alkali environments, the chemical bonds or physical interactions inside traditional hydrogels are liable to be destroyed, causing the corrosion, swelling and even degradation of the hydrogels. Glutaraldehyde is often used to enhance the acid resistance of chitosan *via* covalent crosslinking interactions between the aldehyde groups (–CHO) in glutaraldehyde and the amino groups ($-NH_2$) in chitosan. However, the intrinsic toxic nature of glutaraldehyde in addition to the covalent crosslinking occurring at the expense of amino functional groups of the polysaccharide makes this unfavourable.[44] Our working hypothesis was that the negatively charged POMs would enhance the acid- and base-resistant properties of chitosan hydrogels due to the formation of a strong ionic cross-linking network. To test the acid- and base-resistance properties of the POM@CS hydrogels, the as-prepared hydrogels were soaked in aqueous solutions of different pH for 24 h. These pH assays were carried out for hydrogels prepared from a variety of POMs. The samples exposed to pH 2–10 all maintained their structure and integrity after the 24 h period in acidic or basic solution (Fig. S5†). The appearance of the hydrogels remained unchanged over pH 2–10, and only began to lose their structural integrity at pH < 1 and >12. Dynamic Mechanical Analysis (DMA) was used to study the viscoelastic behaviour of the samples.[45] Fig. 5 was obtained after stress-controlled measurements were taken for $CoSiW_{11}$@CS hydrogel samples after 24 h immersion at pH 2, 7, and 10.

The Young's modulus was obtained from the linear region (0–0.015 strain) of a classical stress–strain curve – measured up to 20% engineering strain – and provides information on the strength or toughness of a material. Fig. S6† contains the resulting graph of the Young's modulus values for each pH value. The Young's modulus values suggest that hydrogels are more resistant to acidic pH than basic pH since their elasticity remained almost unchanged. This likely arises due to protonation of the amino functional groups of the chitosan, which increases hydrogen bonding interactions with POM. At pH 10, whilst the hydrogel retained integrity, its Young's modulus was about 25% lower than it was originally (pH 7).

These results suggest that the strong ionic cross-linking interactions of the POM with the chitosan inhibited the penetration of water molecules into the hydrogels, which significantly improved the structural stability and resistance to deformation of the hydrogel in acidic or basic environments. A study conducted in 2020 by Wei and co-workers showed how POM@CS hydrogels prepared from chitosan/silicotungstate–polyacrylamide possessed adhesive, conductive, and self-healing properties.[46] The adhesive qualities exhibited by these hydrogels was tested against organic and inorganic materials, and was found to promptly adhere to numerous surfaces, from stainless steel to glass, and rubber. Additionally, the POM@CS hydrogels demonstrated antibacterial and self-healing properties. Their antibacterial activity against Gram-negative *E. coli* was demonstrated through zone of inhibition studies, while the self-healing properties were tested *via* dynamic stress cycles. Further, where stress was used to break the physical cross-linking networks the strong physical interactions between the negatively charged POM and the cationic amino groups of the chitosan were found to be reversibly conductive, allowing the networks to reconstruct.

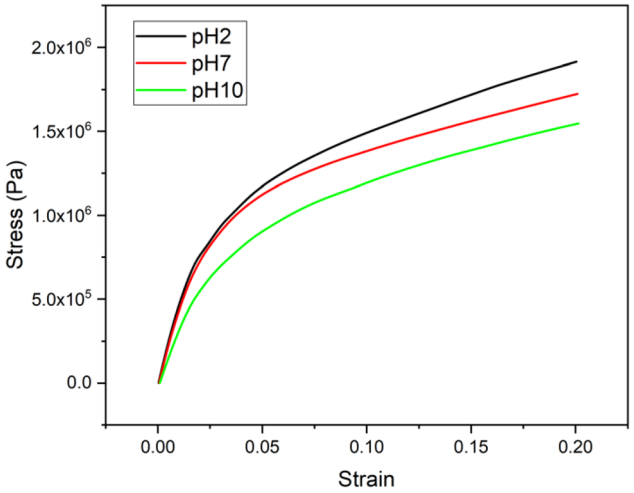

Fig. 5 Stress *vs.* strain curves for hydrogels at pH 2, 7, and 10. The plotted data were averaged from three independent measurements.

Antimicrobial performance of the hydrogels

Embedding essential oils in the $CoSiW_{11}$@CS hydrogel. Several studies have been conducted, exploring the various different materials prepared from POMs and chitosan. One study showed how phosphotungstic acid, $H_3PW_{12}O_{40}$, and phosphomolybdic acid, $H_3PMo_{12}O_{40}$, can be combined with chitosan to form nanocapsules that possessed activity against Gram-negative *Escherichia coli*.[43] Related work demonstrated how gold nanoparticles (AuNPs) can be encapsulated within chitosan hydrogels using phosphotungstic acid as an anionic gelling agent.[47]

The $CoSiW_{11}$@CS hydrogels were doped with the naturally occurring oils, cinnamaldehyde and eugenol, to investigate if the addition of these agents increased the inherent antimicrobial activity exhibited by the gels. Fig. 6 demonstrates how the texture and colour of the hydrogels changed with

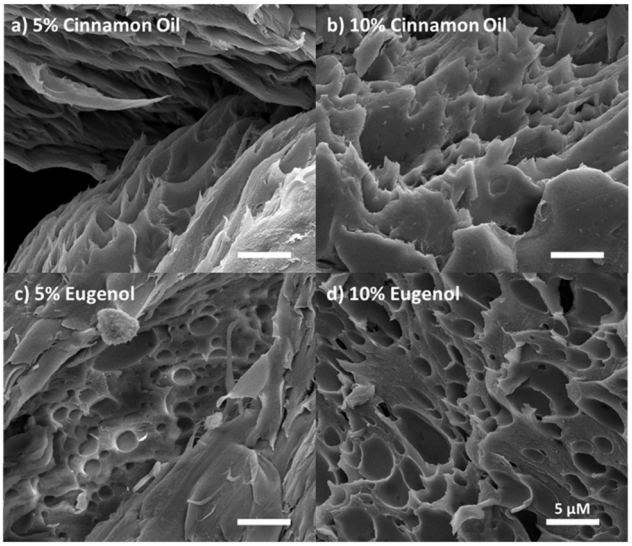

Fig. 6 Eugenol loading in the $CoSiW_{11}$@CS hydrogel. SEM images of cinnamaldehyde- (a and b) and eugenol-loaded (c and d) $CoSiW_{11}$@CS hydrogels.

Table 1 Average values of percentage bacterial reduction of the $CoSiW_{11}$@CS hydrogel (0%) and $CoSiW_{11}$@CS hydrogels loaded with different weight percent of eugenol and cinnamaldehyde

	% bacterial reduction[a]	
% oil	Eugenol *B. subtilis*	Cinnamaldehyde
0%	44	49
2%	43	50
5%	100	100
10%	100	100
	% bacterial reduction[a]	
% oil	Eugenol *E. coli*	Cinnamaldehyde
0%	18	12
2%	19	17
5%	100	100
10%	100	100

[a] Mean values for % bacterial biofilm reduction were calculated from three independent antibiofilm assays.

increasing oil content. The emulsion process and synthesis protocol used to load the hydrogels with oil is demonstrated in Fig. S7.† Inspection of the $CoSiW_{11}$@CS@oil hydrogels using optical microscopy showed the presence of oil droplets within the cross-linked hydrogel matrix (Fig. S8†). Further analysis of oil droplets identified in SEM imaged of the $CoSiW_{11}$@CS@oil hydrogels (Fig. 6) confirmed oil droplets with a mean diameter of 2.30 μm (Fig. S9†).

Evaluation of antibacterial activity. The antibacterial performance of the $CoSiW_{11}$@CS hydrogels was assessed using model Gram-positive and Gram-negative bacterial strains, *B. subtilis* and *E. coli*, respectively. The antibiofilm activity of the hydrogels was assessed using a modification of the Japanese Industrial Standard (JIS) Z 2801 antibiofilm assay.[48] The assay was conducted over three days. The first step involved inoculating the hydrogels and negative control samples with the chosen bacterial inoculum and incubating them overnight, at the appropriate temperature (depending on the bacterial strain being tested). The next day the samples were retrieved and added to a separate Falcon tube containing the suitable culture media. The solutions were then diluted accordingly and 100 μL of the selected dilutions were seeded on agar plates and returned to the incubator overnight to allow for growth of any bacterial colonies. Finally, the number of colony forming units (CFUs) present on each plate were counted. A plastic control sample was used as a reference, and the number of CFUs found on each agar plate associated with that of the hydrogel samples was correlated to the plastic control samples, allowing the bacterial reduction of the hydrogels to be calculated. The results demonstrate how $CoSiW_{11}$@CS hydrogels exhibit antibiofilm activity against both the Gram-positive and Gram-negative model bacterial strains, with greater percentages of bacterial reduction coming in the assays tested against *B. subtilis* (Table 1). In a research reported by Fan and co-workers, the POM@CS hydrogels composed of AgP_5W_{30} and chitosan showed antibacterial activity against *Staphylococcus aureus*, *Escherichia coli*, and methicillin-resistant *Staphylococcus aureus* (MRSA) through zone of inhibition studies.[49]

Meanwhile, the antibacterial activity of the hydrogels doped with cinnamaldehyde and eugenol was also assessed in the same antibiofilm assay (Table 1). Despite the introduction of the oils at 2% content the bacterial reduction of the hydrogels does not improve, however, when the oil content reaches 5 and 10% the bacterial reduction is 100% (Table 1).

The results of the biofilm prevention assays in Table 1 were verified using SEM. Fig. 7 contains SEM of eugenol-loaded $CoSiW_{11}$@CS. Importantly, the samples are unwashed, therefore dead and non-viable *E. coli* cells were still present on the sample surface (indicated by yellow arrows). Briefly, the plastic control sample was covered by a dense layer of *E. coli* colonies, whereas the native $CoSiW_{11}$@CS hydrogel (no eugenol) contained few bacterial cells on the surface, commensurate with the antibacterial properties in Table 1. However, $CoSiW_{11}$@CS doped with eugenol at 5 and 10% content, showed very few *E. coli* cells remaining on the surface, confirming the superior antibacterial activity of the $CoSiW_{11}$@CS@oil hydrogels. Non-viable bacterial colonies and culture media crystals still present on the surface of the samples were removed by washes with distilled sterile water. SEM images following this washing step provide a more representative depiction of the antibacterial properties of each sample (Fig. S8†).

Evaluation of the antifungal activity. The antifungal performance of the $CoSiW_{11}$@CS hydrogel and the $CoSiW_{11}$@CS@oil hydrogels, doped with eugenol and cinnamaldehyde, was tested against two common types of mould,

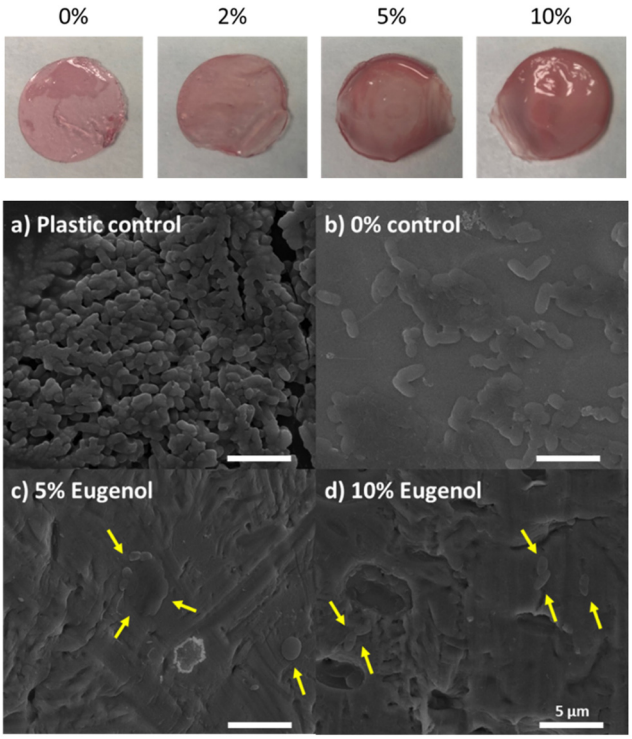

Fig. 7 SEM imaging of *E. coli* biofilm growth on $CoSiW_{11}$@CS hydrogels: (a) plastic control sample, (b) $CoSiW_{11}$@CS hydrogel (0% oil content), and $CoSiW_{11}$@CS hydrogels loaded with eugenol at; (c) 5%, and (d) 10%, after antibiofilm assay, where yellow arrows indicate the few remaining non-viable bacterial cells on the surface of 5 and 10% eugenol samples.

A. niger and *C. cladosporioides* (Fig. S11 and S12†). Glass and plastic surfaces were once again used as negative control samples. Fungal growth was monitored over a six-day period. Both the $CoSiW_{11}$@CS hydrogel and the $CoSiW_{11}$@CS@oil hydrogels displayed potent antifungal activity, where no growth could be observed (Fig. S13†). SEM imaging confirmed these results, where considerable *A. niger* growth was observed on both the glass and plastic samples, whereas $CoSiW_{11}$@CS and $CoSiW_{11}$@CS@oil hydrogels exhibited no fungal growth (Fig. 8). Hydrogels doped with eugenol and cinnamaldehyde at 5 and 10% concentrations (Fig. 9), were also completely clear of any fungal spores, thus suggesting that each hydrogel sample (0, 5 and 10%) exhibited 100% fungal reduction and significant antifungal activity.

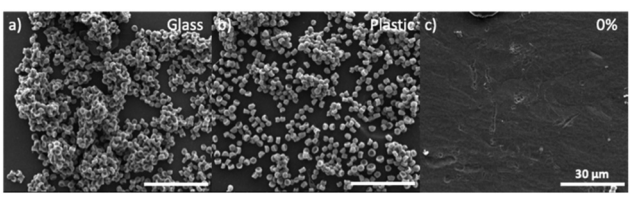

Fig. 8 SEM imaging of *A. niger* growth on the surface of, (a) glass control sample, (b) plastic control sample, and (c) $CoSiW_{11}$@CS hydrogel (with 0% oil content), after the antifungal assay.

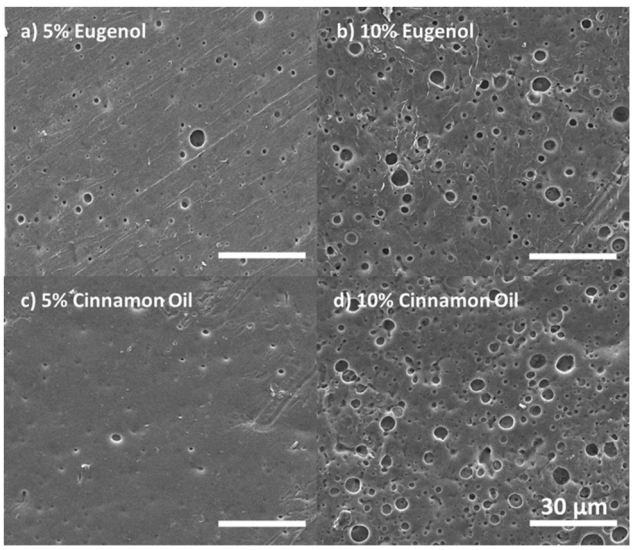

Fig. 9 SEM of $CoSiW_{11}$@CS@oil hydrogels; (a) containing 5% eugenol content, (b) with 10% eugenol content, (c) containing 5% cinnamaldehyde content, and (d) with 10% cinnamaldehyde content, showing no *A. niger* growth, after the antifungal assay.

Experimental

Synthetic procedures

Synthesis of $K_8[\alpha\text{-}SiW_{11}O_{39}]\cdot 12H_2O$. The synthesis is a modification of the literature procedure.[50] $Na_2WO_4\cdot 2H_2O$ (182 g, 0.55 mol) was dissolved in 300 mL of distilled water and the solution was heated to 100 °C (solution A). To the boiling solution A, an aqueous solution of HCl 4 M (165 mL) was added dropwise over 30 min with vigorous stirring in order to dissolve the local precipitate of tungstic acid. Sodium metasilicate (6.1 g, 50 mmol) was dissolved at room temperature in 100 mL of distilled water, followed by the quick addition of aqueous HCl (50 mL, 4 M) (solution B). Solution B was added to solution A and the pH was controlled to 5 by the addition of 1 M KOH, if necessary. The solution was left to boil for 1 h, then left to cool to room temperature overnight, covered with parafilm. The solution was filtered if it was not completely clear. Potassium chloride (150 g) was added, and a colourless precipitate was formed. The solid product was collected on a sintered glass funnel (medium porosity), washed with two 50 mL portions of a potassium chloride solution (1 M), then washed with two 50 mL portions of cold water, and finally dried in air. Yield: 140.67 g (43.9 mmol, 88% based on Si).

Synthesis of $K_6[Co(H_2O)SiW_{11}O_{39}]\cdot 15H_2O$. $K_8[\alpha\text{-}SiW_{11}O_{39}]\cdot 12H_2O$ (3.20 g, 1.00 mmol) was dissolved at room temperature in 30 mL of distilled water (solution C) in a round-bottomed flask. Solution C was heated to 55 °C. In a 50 mL beaker, cobalt chloride (0.136 g, 1.05 mmol) was dissolved, with agitation, in 20 mL of distilled water (solution D). Once solution C reached 55 °C, solution D was added to the round-bottomed flask. The pH was controlled to approximately 5–5.5 by the addition of NaOH (0.1 mol) and was left under magnetic stir-

ring for 90 min. After the stirring period, the solution was filtered using a Buchner funnel and dried under vacuum. The crystals were left overnight, to dry completely. Yield: 1.30 g (0.38 mmol, 38% based on Si).

Preparation of $CoSiW_{11}$@CS hydrogels. In a 15 mL Falcon tube, 0.1619 g of $K_6[Co(H_2O)SiW_{11}O_{39}]\cdot 15H_2O$ single crystals were dissolved in 10 mL of distilled water to obtain a 5 mM solution of $K_6[Co(H_2O)SiW_{11}O_{39}]\cdot 15H_2O$. Separately, in a 50 mL Falcon tube, 1.4 g of chitosan was dissolved in 40 mL of distilled water to give a solution of 35 mg mL^{-1} (pH 6.5). The solution was mixed using a glass stirring rod, then incubated at 70 °C, for 10 min. 457 μL glacial 0.2 M acetic acid was added to the chitosan solution (pH 5.5) and the Falcon tube was returned to the incubator at 70 °C, overnight. In a 24 well-plate, 500 mg of chitosan solution was added to the required number of wells. $K_6[Co(SiW_{11}O_{39})]\cdot 15H_2O$ solution (500 μL, 5 mM) was added down the side of each well, towards the chitosan solution, and was left to gel overnight.

Preparation of $CoSiW_{11}$@CS@oil hydrogels. Eugenol and cinnamaldehyde emulsions were prepared in a 5 mL Eppendorf vial at concentrations of 2, 5, and 10% (100 μL of oil and 4.9 mL of chitosan solution, 250 μL of oil and 4.75 mL of chitosan solution, and 500 μL of oil and 4.5 mL of chitosan solution). A sonic tip (Hielscher UP400St Ultrasonic Processor, operating at 100 W and 50% amplitude) was used for room temperature emulsification over a period of 10–20 s. The preparation of $CoSiW_{11}$@CS@oil hydrogels was identical to the $CoSiW_{11}$@CS hydrogels, replacing the chitosan solution with the corresponding freshly prepared oil-in-chitosan emulsion. FT-IR (cm^{-1}): 3300 (O–H and N–H stretching), 1600 (–NH_2 and H_2O), 1400 (–CH_2–), 1375 (–CH_3), 1100 (antisymmetric C–O–C stretching and C–N stretching), 990 (W═O), 950 (W–O), and 900 (W–O–W).

Characterisation methods

Scanning electron microscopy (SEM) imaging of hydrogels

SEM visualisation of $CoSiW_{11}$@CS and $CoSiW_{11}$@CS@oil hydrogels. The hydrogels were dried by supercritical drying and were coated with Au/Pd. The dried/coated samples were then visualised on an Inspect F50A electron microscope operating at 30 kV.

SEM visualisation of E. coli growth on hydrogel surfaces. The hydrogels were coated with 14 nm of palladium. The coated samples were then visualised on an Inspect F50A electron microscope operating at 30 kV.

SEM visualisation of A. niger proliferation on hydrogel surfaces. The fixation protocol was performed as follows: the samples were deposited in a 6-well plate and washed with saline, by adding 2 mL to each well. The saline solution was then removed after a few seconds of agitation. 2 mL of 0.1 M cacodylate buffer was then added to each well, and the plate was incubated for 90 min at 37 °C. The buffer was then removed, and the samples were washed in increasing concentrations of methanol (2 mL per well) to dehydrate the moulds, 5 min with MeOH at 30%, 5 min with MeOH at 50%, 5 min with 70% methanol, 10 min with 100% methanol, and then another 5 min with 100% methanol. Each step was carried out twice. The hydrogels were coated with carbon. The fixed and coated samples were then visualised on a Quanta FEG-250 (FEI Company) field emission SEM for high-resolution imaging operating at 30 kV.

Transmission electron microscopy (TEM) imaging of hydrogels. TEM images were acquired by depositing hydrogel samples on a TEM grid and visualising them using bright-field imaging in an FEI Tecnai T20 microscope operating at 200 kV.

pH resistance assays. Hydrogels were prepared in 5 × 3 cm rectangular moulds with 4.0 g of chitosan solution and 3 mL of $K_6[Co(H_2O)SiW_{11}O_{39}]\cdot 15H_2O$ solution. The gels were then cleaned using distilled water and submerged in 150 mL of the solution of either pH 2, 4, 7, 10 or 12, for 24 hours. The acidic solutions were prepared from H_2SO_4 (98% w/w), the pH 7 solution was distilled water, and the basic solutions were prepared from a 3 M stock solution of NaOH. 0.01 M sulfuric acid was used as the pH 2 solution, with the pH 4 solution prepared from 0.0001 M of H_2SO_4. Similarly, the pH 10 solution was prepared from 0.0001 M of sodium hydroxide, whereas the solution of pH 12 was 0.01 M NaOH. The pH was monitored using a pH meter, accurate to two decimal places.

Dynamic mechanical analysis (DMA). Tensile tests were performed with DMA 450+ (Fa. MetraviB). From the prepared hydrogels test specimens were cut with a scalpel from these larger hydrogel samples. Specimens for measurement had the following dimensions: width: 10 mm, length of about 30 mm. The free length between clamps was 20 mm, sample thickness was approximately 0.1 mm (specified for each individual test specimen to precision of ±0.02 mm). From each larger hydrogel sample preparation, three individual specimens were prepared and measured, and the plotted data were averaged from these three independent measurements.

The test conditions of the tensile tests were as follows. Tensile deformation was applied by controlling a force-ramp of 0.01 N s^{-1} over the test-time, measuring the resulting extension of the sample due to the applied tensile force. The machine has a displacement resolution of 0.1 μm. Data points were taken about each 1 μm of displacement variation.

The test specimens were tested under "wet-conditions" so as to ensure that the samples had and maintained their hydration level during measurement. Evaporation of humidity was not controlled directly, but all sample preparation and tests were executed at room temperature (controlled conditions 23.0 ± 2.0 °C; controlled relative humidity 50%). Test duration was about 5 min from starting to cut the specimen to finish of the tensile test. Therefore, effects on the mechanical measurements due to varying hydration levels are unlikely.

Surface-active antimicrobial activity of the hydrogels

Bacterial biofilm prevention assays. Two strains of bacteria were tested in the antibiofilm assays: Gram-positive *Bacillus subtilis* 1904-E and Gram-negative *Escherichia coli* DH5α. Bacterial passages were performed the day prior to the assay, in which 500 μL of *B. subtilis* or *E. coli* was pipetted into a flask containing 9.5 mL of Nutrient Broth (NB), for *B. subtilis*, or Lysogeny Broth (LB), for *E. coli* culture media, to allow fresh bacterial growth.

The antibacterial activity of the various hydrogels and plastic control samples was tested against *B. subtilis* and *E. coli*. 500 μL of the selected bacteria was added to 9.5 mL of either NB or LB culture media in a Falcon, and vortexed to homogenise the inoculum. The hydrogels were placed in an empty Petri dish, sterilised under UV light for 5 min, then inoculated with 50 μL of the 10^6 CFU per mL inoculum, and incubated at 37 °C for 24 h in a humidity chamber. After the incubation time, the samples were removed from the humidity chamber and 20 mL of the appropriate culture media was added to a Falcon for each sample. Each gel/control sample was carefully placed into their respective Falcon and vortexed for 1 min. The contents of the Falcon were then diluted by a factor of 10 using culture media, and 100 μL of the appropriate dilutions were then added to an agar plate using a micropipette. 2 mm sterile glass beads were then added to each plate, agitated thoroughly to spread the bacteria around the plate, and disposed of in bleach. Parafilm was used to secure the lid to each plate, and they were incubated at 37 °C for 24 h. After the incubation period, the plates were removed, the colony forming units were counted and recorded in a table, and bacterial reduction percentage values were calculated.

Antifungal activity assays. Two moulds were tested in the antifungal assays: *Aspergillus niger* CECT 2088 and *Cladosporium cladosporioides* CECT 2111. For the fungal adhesion assays, the following liquid medium was used: 2.0 g L^{-1} KH_2PO_4; 1.4 g L^{-1} $(NH_4)_2SO_4$; 0.0027 g L^{-1} $FeSO_4{\cdot}7H_2O$; 0.0016 g L^{-1} $MnSO_4{\cdot}H_2O$; 0.0014 g L^{-1} $ZnSO_4{\cdot}H_2O$; 0.0037 g L^{-1} $CoCl_2{\cdot}6H_2O$; 0.6 g L^{-1} $MgSO_4{\cdot}7H_2O$; 0.4 g L^{-1} $CaCl_2{\cdot}2H_2O$; 0.75 g L^{-1} peptone; 2.0 g L^{-1} Tween 80; 0.3 g L^{-1} urea; and 5 g L^{-1} glucose in formate buffer 50 mM pH = 4.8. Fungal spore suspensions were stored in 0.1% Tween, 20% glycerol at −80 °C prior to use. Before each assay, fungal cells were inoculated in SDA plates and slants (Sabouraud Dextrose Agar (supplemented with chloramphenicol, Scharlab, S.L.)) and *A. niger* grown at 35 °C for 4 days, and *C. cladosporioides* grown at 25 °C for 4 days.

Fungal spores were incubated for four days in SDA plates at 35 °C for *A. niger* and at 25 °C for *C. cladosporioides*. 2 mL of distilled H_2O with 0.1% Tween was added to the slant, containing the fungus, and the slant was agitated to allow the spores to pass into the solution. The solution was then transferred to a 5 mL Eppendorf followed by 3 mL of distilled H_2O with 0.1% Tween, to dilute the solution. The Eppendorf was then vortexed for 15 seconds, to allow thorough dispersion of the spores in the solution. The inoculum was prepared at 10^6 conidia per mL and the absorbance was measured at 620 nm, using a plastic cuvette, with the desirable absorbance in the range 0.09–0.11. The solution was then diluted by a factor of ten, three times, using 200 μL of the inoculum and 1800 μL of RPMI. The final concentration of the inoculum was 10^3 conidia per mL.

The hydrogel and plastic/glass (2 × 2 cm) control samples were placed into a 6-well plate and sterilised under UV light for 5 minutes. 100 μL of the 10^3 conidia per mL in RPMI inoculum was then added to the surface of each sample, and the well plates were placed into a humidity chamber and incubated at the appropriate temperature (25 °C/35 °C) for 24 h. The samples were observed over the next six days, whereupon the mould growth/lack of mould growth was noted.

Conclusions

Self-assembled organic–inorganic hybrid structures increase the possibilities for a material to foster properties which differ from their non-assembled component parts. In this investigation, a solid and resistant hydrogel material was synthesised from mono-lacunary Keggin-type polyoxometalates, such as $K_6[Co(H_2O)SiW_{11}O_{39}]$, and the biocompatible polymer, chitosan. Electron microscopy and viscoelastic analysis revealed the fibrous nature of the $CoSiW_{11}$@CS hydrogels, which maintained their structural integrity over a broad range of pH, from pH 2–10. In addition, the self-assembled hydrogels exhibited broad-spectrum surface-active antimicrobial activity, which could be enhanced by incorporating bioactive compounds – eugenol and cinnamaldehyde – into the organic–inorganic matrix during synthesis. Overall, the physicochemical and biological properties of these hydrogels render them relevant to a range of potential applications, including antimicrobial stick-to-skin wound healing patches and composite membrane materials for the purification of water, or as acid- and base-resistant coatings as well as innovative antifouling materials to prevent microbiologically-influenced corrosion (MIC). In addition to exploring their use in such applications, our ongoing research into these materials will involve characterising how the electron transfer and storage capabilities of the POM might afford specific catalytic properties to the material and how these properties can be modulated through chemical bonding with the chitosan polymer.

Author contributions

Conceptualisation – SGM; methodology – IFC, ASA, & SGM; investigation – CMcW, IFC, ASA, & SGM; data curation – all the authors; writing, original draft – CMcW & SGM; writing, review & editing – SGM; supervision; SGM & IFC. Project administration; SGM & RMR; funding acquisition – SGM & RMR.

Conflicts of interest

There are no conflicts to declare.

Acknowledgements

This work was funded through the grant PID2022-141276OB-I00 funded by MCIN/AEI/10.13039/501100011033 (Ministerio de Ciencia e Innovación/Agencia Estatal de Investigación, Spain) and was supported by MCIN with funding from European Union NextGenerationEU (PRTR-C17.

I1) promoted by the Government of Aragón. The authors also acknowledge Fondo Social del Gobierno de Aragón (grupo DGA E15_23R) and Programa Operativo Aragón de Fondo Social Europeo 2014-2020 (I. F. C.). The authors acknowledge the Servicio General de Apoyo a la Investigación-SAI (Universidad de Zaragoza), for the use of instrumentation as well as the technical advice provided by the National Facility ELECMI ICTS, node "Laboratorio de Microscopías Avanzadas" at University of Zaragoza.

References

1 WHO, 68th World Health Assembly, 2015, **https://apps.who.int/gb/ebwha/pdf_files/WHA68-REC1/A68_R1_REC1-en.pdf**.
2 WHO, Call to Action on Antimicrobial Resistance, 2021, **https://www.who.int/news/item/30-07-2021-call-to-action-on-antimicrobial-resistance-2021**.
3 M. Dryden, A. P. Johnson, D. Ashiru-Oredope and M. Sharland, *J. Antimicrob. Chemother.*, 2011, **66**, 2441.
4 T. M. Rawson, D. Ming, R. Ahmad, L. S. P. Moore and A. H. Holmes, *Nat. Rev. Microbiol.*, 2020, **18**, 409.
5 N. Chen, *et al.*, *Lancet*, 2020, **395**, 507.
6 F. Zhou, *et al.*, *Lancet*, 2020, **395**, 1054.
7 A. L. Frantz, *Toxicol. Environ. Health Sci.*, 2023, **15**, 199.
8 M. C. Jennings, K. P. C. Minbiole and W. M. Wuest, *ACS Infect. Dis.*, 2015, **10**, 288.
9 S. E. Al-Khalifa, M. C. Jennings, W. M. Wuest and K. P. C. Minbiole, *ChemMedChem*, 2017, **12**, 280.
10 S. Alkhalifa, M. C. Jennings, D. Granata, M. Klein, W. M. Wuest, K. P. C. Minbiole and V. Carnevale, *ChemBioChem*, 2020, **21**, 1510.
11 J. M. Tennent, B. R. Lyon, M. T. Gillespie, J. W. May and R. A. Skurray, *Antimicrob. Agents Chemother.*, 1985, **27**, 79.
12 K. P. C. Minbiole, M. C. Jennings, L. E. Ator, J. W. Black, M. C. Grenier, J. E. LaDow, K. L. Caran, K. Seifert and W. M. Wuest, *Tetrahedron*, 2016, **72**, 3559.
13 B. R. Lyon and R. Skurray, *Microbiol. Rev.*, 1987, **51**, 88.
14 A. Abuzaid, A. Hamouda and S. G. B. Amyes, *J. Hosp. Infect.*, 2012, **81**, 87.
15 S. Mayer, M. Boos, A. Beyer, A. C. Fluit and F.-J. Schmitz, *J. Antimicrob. Chemother.*, 2001, **47**, 896.
16 W. J. Liu, L. Fu, M. Huang, J. P. Zhang, Y. Wu, Y. S. Zhou, J. Zeng and G. X. Wang, *J. Med. Microbiol.*, 2017, **66**, 13.
17 S. Ignak, Y. Nakipoglu and B. Gurler, *Antimicrob. Resist. Infect. Control*, 2017, **6**, 88.
18 B. Chen, J. Han, H. Dai and P. Jia, Biocide-tolerance and antibiotic-resistance in community environments and risk of direct transfers to humans: Unintended consequences of community-wide surface disinfecting during COVID-19, *Environ. Pollut.*, 2021, **283**, 117074, ISSN: 0269-7491.
19 K. Kainz, M. A. Bauer, F. Madeo and D. Carmona-Gutierrez, *Microb. Cell*, 2020, **7**, 143.
20 M. C. Fisher, *et al.*, *Nat. Rev. Microbiol.*, 2022, **20**, 557.
21 A. K. Gupta, M. Venkataraman, H. J. Renaud, R. Summerbell, N. H. Shear and V. Piguet, *Int. J. Dermatol.*, 2021, **60**, 474.
22 F. Bongomin, S. Gago, R. O. Oladele and D. W. Denning, *J. Fungi*, 2017, **3**, 57.
23 G. D. Brown, D. W. Denning, N. A. R. Gow, S. M. Levitz, M. G. Netea and T. C. White, *Sci. Transl. Med.*, 2012, **4**, 165rv13.
24 The WHO fungal priority pathogens list, 2022, **https://www.who.int/publications/i/item/9789240060241**.
25 L. Cronin and A. Müller, *Chem. Soc. Rev.*, 2012, **41**, 7333.
26 S.-S. Wang and G.-Y. Yang, *Chem. Rev.*, 2015, **115**, 4893.
27 S. Lentink, D. E. Salazar Marcano, M. A. Moussawi and T. N. Parac-Vogt, *Angew. Chem., Int. Ed.*, 2023, **62**, e202303817.
28 J. Liu, M. Huang, X. Zhang, Z. Hua, Z. Feng, Y. Dong, T. Sun, X. Sun and C. Chen, *Coord. Chem. Rev.*, 2022, **472**, 214785.
29 A. Misra, I. Franco Castillo, D. Müller, C. González, S. Eyssautier-Chuine, A. M. Ziegler, J. M. de la Fuente, S. G. Mitchell and C. Streb, *Angew. Chem., Int. Ed.*, 2018, **57**, 14926.
30 K. Rajkowska, A. Koziróg, A. Otlewska, M. Piotrowska, E. Atrián-Blasco and S. G. Mitchell, *Molecules*, 2020, **25**, 5663.
31 A. G. Enderle, I. Franco-Castillo, E. Atrián-Blasco, R. Martín-Rapún, L. Lizarraga, M. Culzoni, M. Bollini, J. M. de la Fuente, F. Silva, C. Streb and S. G. Mitchell, *ACS Appl. Polym. Mater.*, 2022, **4**, 4144.
32 I. Franco-Castillo, A. Misra, S. Laratte, M. Gommeaux, R. Perarnau, N. Vaillant-Gaveau, J. Pierlot, C. Streb, S. G. Mitchell and S. Eyssautier-Chuine, *Int. Biodeterior. Biodegrad.*, 2022, **173**, 105459.
33 S. Eyssautier-Chuine, I. Franco-Castillo, A. Misra, J. Hubert, N. Vaillant-Gaveau, C. Streb and S. G. Mitchell, *Sci. Total Environ.*, 2023, **884**, 163739.
34 H. Soria-Carrera, E. Atrián-Blasco, R. Martín-Rapún and S. G. Mitchell, *Chem. Sci.*, 2023, **14**, 10.
35 H. Soria-Carrera, I. Franco-Castillo, P. Romero, S. Martín, J. M. de la Fuente, S. G. Mitchell and R. Martín-Rapún, *Angew. Chem., Int. Ed.*, 2021, **60**, 3449.
36 H. Soria-Carrera, E. Atrián-Blasco, J. M. de la Fuente, S. G. Mitchell and R. Martín-Rapún, *Nanoscale*, 2022, **14**, 5999.
37 S. M. Joseph, S. Krishnamoorthy, R. Paranthaman, J. A. Moses and C. Anandharamakrishnan, *Carbohydr. Polym. Technol. Appl.*, 2021, **2**, 100036.
38 S. Peers, A. Montembault and C. Ladavière, *Carbohydr. Polym.*, 2022, **275**, 118689.
39 I. Serrano-Sevilla, Á. Artiga, S. G. Mitchell, L. De Matteis and J. M. de la Fuente, *Molecules*, 2019, **24**, 2570.
40 Á. Artiga, S. García-Embid, L. De Matteis, S. G. Mitchell and J. M. de la Fuente, *Front. Chem.*, 2018, **6**, 234.
41 S. Mukhopadhyay, J. Debgupta, C. Singh, A. Kar and S. Das, *Angew. Chem.*, 2018, **130**, 1936.
42 Z. Wang, X. Xin, M. Zhang, Z. Li, H. Lv and G. Y. Yang, *Sci. China: Chem.*, 2022, **65**, 1515.

43 L. De Matteis, S. G. Mitchell and J. M. de la Fuente, *J. Mater. Chem. B*, 2014, **2**, 7114.
44 J. Wu, Z. Dong, X. Li, P. Li, J. Wei, M. Hu, L. Geng and X. Peng, *J. Environ. Chem. Eng.*, 2022, **10**, 107754.
45 K. Dyamenahalli, A. Famili and R. Shandas, *Shape Memory Polymers for Biomedical Applications*, Woodhead Publishing, 2015, pp. 35–63, ISBN: 9780857096982.
46 X. Wei, K. Ma, Y. Cheng, L. Sun, D. Chen, X. Zhao, H. Lu, B. Song, K. Yang and P. Jia, *ACS Appl. Polym. Mater.*, 2020, **2**, 2541.
47 Á. Artiga, F. Ramos-Sánchez, I. Serrano-Sevilla, L. De Matteis, S. G. Mitchell, C. Sánchez-Somolinos and J. M. de la Fuente, *Part. Part. Syst. Charact.*, 2020, **37**, 2070011.
48 W. van Rensburg, W. Laubscher and M. Rautenbach, *MethodsX*, 2021, **8**, 101593.
49 B. Fan, N. Cui, Z. Xu, K. Chen, P. Yin, K. Yue and W. Tang, *Biomacromolecules*, 2022, **23**, 972.
50 A. P. Ginsberg, *Inorganic Syntheses*, Wiley, 1990, vol. 27, ISBN: 9780471509769.